PAPER • **OPEN ACCESS**

Unveiling the potential of 3D TH-graphyne: a porous carbon anode for efficient potassium-ion storage

To cite this article: Arzoo Hassan *et al* 2025 *Phys. Scr.* **100** 115930

Physica Scripta

OPEN ACCESS

RECEIVED
25 July 2025

REVISED
2 October 2025

ACCEPTED FOR PUBLICATION
31 October 2025

PUBLISHED
13 November 2025

PAPER

Unveiling the potential of 3D TH-graphyne: a porous carbon anode for efficient potassium-ion storage

Arzoo Hassan[1], **Marcelo L Pereira Junior**[2], **L Shaw**[3], **Umer Younis**[4] and **Dongyang Li**[1,*]

[1] Department of Chemical and Materials Engineering, University of Alberta, Edmonton, AB, T6G 2H5, Canada
[2] Department of Electrical Engineering, College of Technology, University of Brasília, Brasília, Federal District, Brazil
[3] Department of Mechanical, Materials and Aerospace Engineering, Illinois Institute of Technology, Chicago, IL, United States of America
[4] Department of Chemistry, Southern University of Science and Technology, Shenzhen, Guangdong, People's Republic of China
[*] Author to whom any correspondence should be addressed.

E-mail: dongyang.li@ualberta.ca

Keywords: porous carbon nanomaterials, potassium-ion batteries, anode materials, 3D materials

Supplementary material for this article is available online

Abstract

Due to the abundance and low cost of potassium resources, potassium-ion batteries have emerged as promising alternatives to Li-ion batteries, with high capacity and fast ion transport. This study presents a novel three-dimensional triangular-hexagonal graphyne-like (3D TH-GY) carbon allotrope engineered by incorporating acetylenic linkers. *Ab initio* calculations confirm that the semi-metallic 3D TH-GY is thermally and dynamically stable, having a small bandgap of 0.04 eV. The electrochemical potential of 3D TH-GY, along with a recently proposed two-dimensional porous carbon allotrope (TH-GY), is assessed as an anode material for KIBs via DFT calculations. The study reveals strong K-ion binding, with values of –0.97 eV for 2D TH-GY and –1.53 eV for 3D TH-GY, respectively, facilitating efficient ion intercalation while ensuring favorable desorption kinetics. The calculated diffusion barriers for K-ion migration are exceptionally low (0.036 eV for 2D TH-GY, 0.12 eV for 3D TH-GY), indicating rapid ion transport across the surface. Moreover, the theoretical capacities of 2D TH-GY and 3D TH-GY reach 929.83 and 495.91 mAh g^{-1}, respectively, positioning them as promising candidates for high-performance charge–discharge cycles in KIBs. The combination of high charge storage capacity, fast ion diffusion, and structural robustness highlights TH-GY-based materials as compelling alternatives for next-generation potassium-ion battery anodes.

Introduction

The increasing global demand for fossil fuel resources necessitates the development of alternative energy sources and advanced energy storage technologies [1–3]. Among them, lithium-ion batteries (LIBs) have dominated the energy storage market due to lithium's advantageous properties, including a wide operating voltage, high capacity, excellent cyclic stability, superior energy density, and reversible electrochemical behavior [4–6]. However, LIBs face challenges such as lithium scarcity, high costs, safety risks, and the environmental impact of organic electrolytes [7–10]. As a result, there has been growing interest in alternative ion-based batteries, such as potassium-ion batteries (KIBs), which benefit from the abundance and lower cost of potassium resources [9, 11]. Despite these advantages, developing suitable anode materials for KIBs remains a significant challenge due to the large ionic radius of K^+ (1.38 Å, compared to 0.76 Å for Li^+), which causes slow diffusion, structural degradation, and limited electrochemical performance. Thus, developing new carbon allotropes capable of efficiently accommodating K^+ ions while maintaining structural stability and high storage capacity has become a significant research area.

Carbon-based materials have been widely explored for energy storage due to their superior properties, high surface-to-volume ratio [12], structural versatility [13–16], and diverse electronic properties [17–21]. Graphite (372 mAh g^{-1}) and graphidyne (744 mAh g^{-1}) (LiC_3) have been studied as anode materials [22, 23] and their limitations in accommodating large ions have led to research into novel 2D carbon allotropes, including Net-Γ [21], Ψ-graphene [18], Net-W [24], C_{18} [25], C_{36} [25], popgraphene [26], Irida-graphene [27], and germa-graphene [28]. Among the current focus areas in battery research, metallic carbon materials have garnered significant attention due to their unique properties, including negative differential resistance [29], phonon-plasmon coupling [30], catalysis [31], and superconductivity [32]. Recent breakthroughs in carbon allotrope synthesis, such as gamma-graphyne (γ-GY) and the Biphenylene Network (BPN), a system proposed decades ago and synthesized in 2021 by Fan and collaborators, have demonstrated the feasibility of designing porous carbon frameworks [33]. New structures incorporating acetylenic linkages, such as Tolanene [34] and THD-C [35] have further expanded this field.

Triangular-Hexagonal-Graphyne (TH-GY) follows a similar approach to rγ-GY but enforces connections via acetylenic groups between hexagons using only four branches [36], increasing system porosity and creating a highly rigid triangular ring structure. This unique architecture enhances conductivity and ion diffusion, making TH-GY a promising candidate for KIB anodes. Given the challenges of accommodating large K^+ ions while maintaining structural stability, this study investigates the electrochemical behavior and storage capacity of 2D and 3D TH-GY as novel anode materials for K-ion batteries.

In this work, for the first time, a 3D porous carbon structure, termed 3D TH-GY, was designed with acetylenic linkers positioned out of the TH-GY plane, providing many active sites for metal ions adsorption. The results obtained from density function theory (DFT) calculations reveal that the 3D TH-GY is dynamically and thermally stable, with a semi-metallic nature revealed by electronic band structure calculations. This study addresses the key questions: compared with conventional carbon-based anodes, can 3D TH-GY and previous 2D base-structure as well achieve high reversible capacity and fast ion diffusion while retaining structural stability during charge–discharge cycles? Our findings help explore the potential of this type of novel material to outperform conventional carbon-based anodes and offer insights into its applications for next-generation energy storage systems.

Methodology

All calculations were performed using the density functional theory (DFT) within the Vienna Ab-*initio* Simulation Package (VASP) [37]. All the calculations are performed on a 2 × 2 supercell of 2D TH-GY. The projector augmented wave (PAW) method was employed for electron–ion interactions, and the Perdew–Burke–Ernzerhof (PBE) functional was used for exchange–correlation effects [38]. A plane wave energy cutoff of 500 eV and a vacuum layer of 15 Å were applied to avoid interaction between periodic images. Geometric optimization was conducted using the conjugate gradient method with convergence criteria of 10^{-5} eV for energy and 10^{-3} eV $Å^{-1}$ for forces. The electronic band structure was computed using the HSE06 hybrid functional with a Monkhorst–Pack grid of 12 × 12 × 1 [39]. Van der Waals (vdW) interactions were included via Grimme's D2 method [40]. Bader charge analysis was used to examine charge transfer [41]. In the meantime, the climbing-image nudged elastic band (CI-NEB) method was applied to calculate the K-ion diffusion barrier by identifying the transition state when the K-ion migrated in the selected pathways, enabling the calculation of the diffusion barrier in TH-GY [42]. The force convergence criterion for CI-NEB was set at 0.03 eV $Å^{-1}$. *Ab initio* molecular dynamics (AIMD) [43] simulations are conducted to verify the thermal stability along the canonical ensemble. To verify the dynamic stability of this novel structure, we calculated the phonon spectrum by employing the finite displacement method as implemented in the Phonopy code [44].

Results and discussion

The geometry of the newly proposed TH-GY [36] (see figure S1(a)) was designed by combining triangular (T) and hexagonal (H) carbon rings, covalently interconnected through acetylenic linkers, resulting in a 2D porous carbon allotrope. The high porosity and large surface area of TH-GY, coupled with its intrinsic metallic behavior, make it a promising candidate for energy storage applications, particularly as an anode material for KIBs. A comprehensive structural analysis of TH-GY and its comparison with other carbon allotropes are provided in table S1, while its phonon and thermal stability are confirmed in figures S1(b), (c).

Extending this concept to three dimensions, 3D TH-GY was constructed by acetylenic linkers positioned out of the TH-GY plane. However, determining the optimal configuration of these linkers presented a significant challenge. If arranged entirely out-of-plane, connecting acetylenic groups within the plane would disrupt their sp-hybridization. Conversely, if placed adjacent to the in-plane acetylenic groups linking the

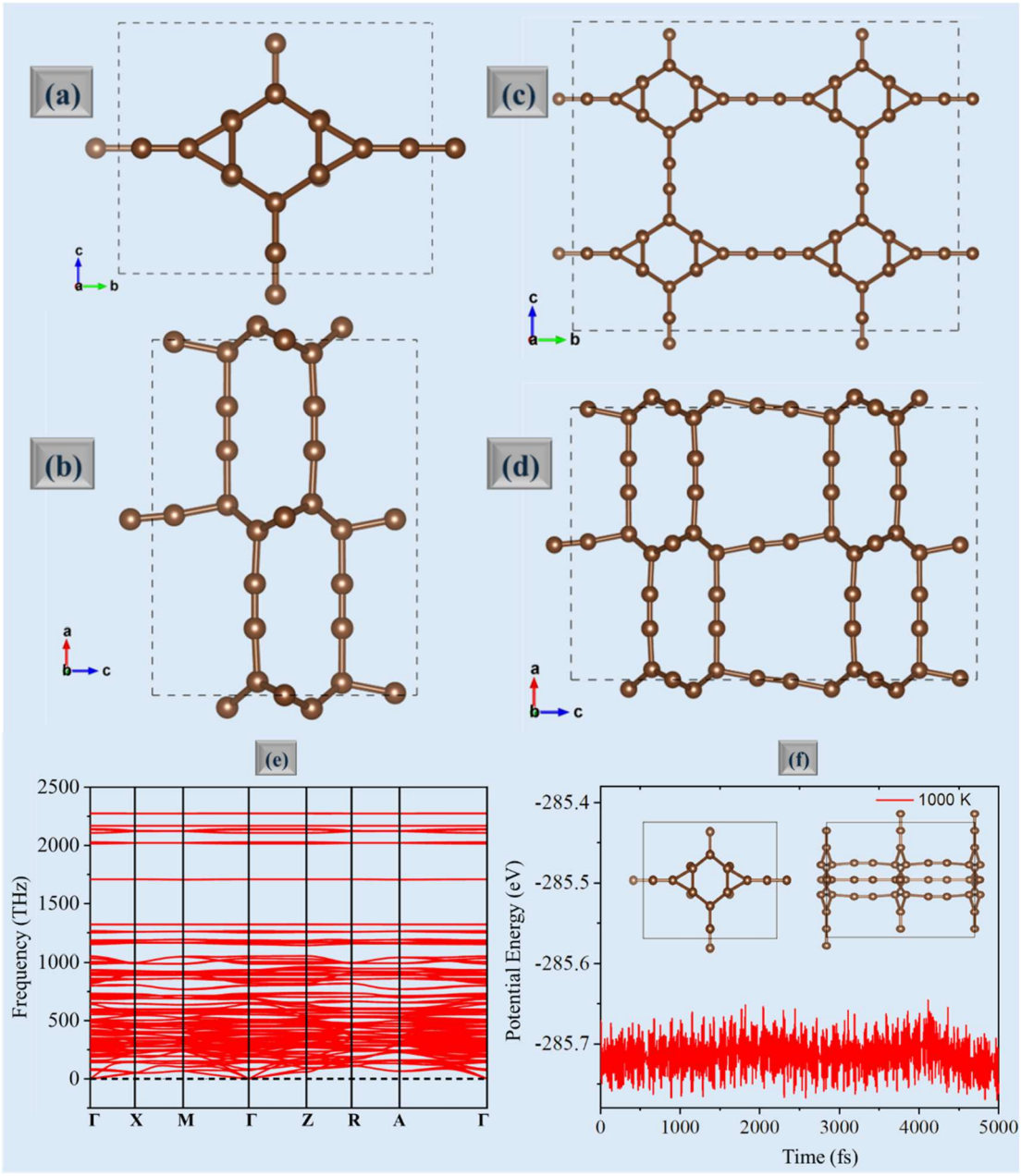

Figure 1. Top (a) and side (b) views of the fully relaxed geometry of unit cell 3D TH-GY. Top (c) and side (d) views of fully relaxed geometry of 2 × 2 × 1 supercell 3D TH-GY; Dynamic and thermal stability of 3D TH-GY: (e) Phonon spectrum and (f) temporal evolution of potential energy during a 5 ps *ab initio* molecular dynamics simulation. The inset panels depict the nanomaterial at the final moment of the AIMD simulation.

triangular rings, the structural rigidity of the 3D framework would be compromised due to the valency constraints of the carbon atoms. To circumvent these limitations, we designed the final structure by interleaving the out-of-plane linkers in alternating directions along the TH-GY hexagonal rings, yielding the 3D TH-GY architecture — a 3D carbon allotrope with sp-sp [2]-sp [3] hybridization, in which acetylenic pairs along all principal crystallographic directions interconnect benzene rings (figures 1(a)–(d)).

The primitive unit cell of 3D TH-GY comprises 36 atoms, adopting an orthorhombic lattice with a Pmmm space group. The optimized lattice parameters are a = 9.725 Å, b = 9.049 Å, and c = 7.257 Å. Seven distinct bond types are identified within the structure: bond lengths within the triangular rings are 1.48 Å, while those in the hexagonal rings measure 1.44 Å. The bonds linking triangular and hexagonal rings are shorter (1.16 Å). Additionally, the central bonds within the acetylene and diacetylene linkages, which bridge the triangular and hexagonal units, have lengths of 1.21 Å and 1.28 Å, respectively. These features define a highly porous structure, where the arrangement of triangular and hexagonal rings dictates the pore sizes. Given this unique architecture, 3D TH-GY is expected to exhibit mechanical adaptability, making it a strong candidate for ion battery applications.

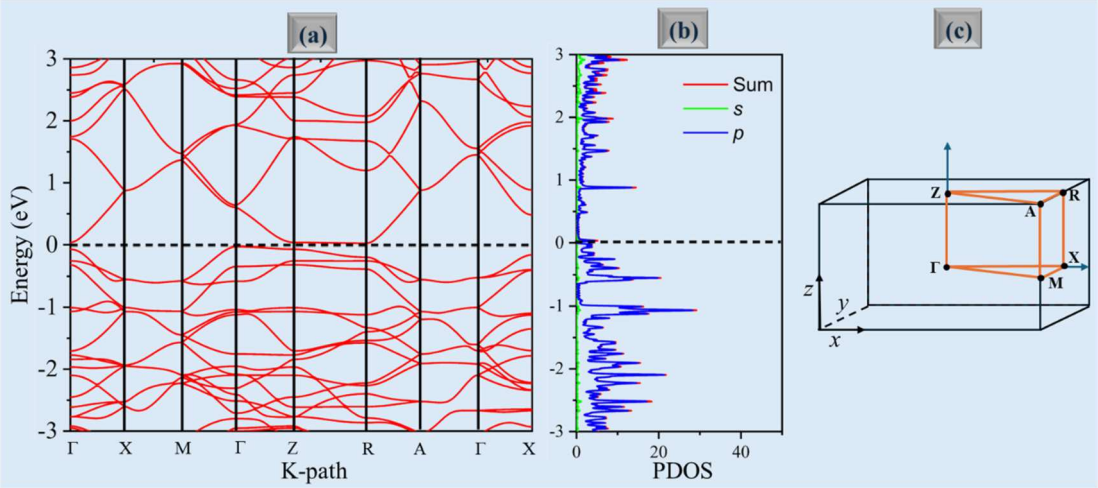

Figure 2. Electronic band structure (a), PDOS (b), and high symmetry k-path (c) of 3D TH-GY.

To evaluate the stability of the 3D TH-GY monolayer, we computed its phonon spectrum using the PHONOPY code within a $2 \times 2 \times 1$ supercell. As shown in figure 1(e), the phonon dispersion confirms the dynamic stability of the porous structure, with no imaginary frequencies throughout the Brillouin zone. Flat bands around 2250 cm^{-1} are attributed to the vibrational modes of sp-hybridized carbon atoms.

Additionally, the thermal stability of metallic 3D TH-GY was assessed via *ab initio* molecular dynamics (AIMD) simulations performed at 1000 K over a 5 ps timescale within a $1 \times 2 \times 2$ supercell. The AIMD results in figure 1(f) demonstrate that 3D TH-GY retains its structural integrity at high temperatures, exhibiting only minor fluctuations in potential energy, further validating its thermal robustness.

Electronic properties

We employed the HSE06 hybrid functional to assess electronic properties, including the band structure and partial density of states (PDOS), of both 2D and 3D TH-GY. As shown in Fig. S2(a), the band structure reveals the absence of a band gap between the conduction and valence bands, with clear overlap at the Fermi level, confirming the metallic nature of TH-GY. Figure 2 shows that 3D TH-GY is semi-metallic with a small band gap of approximately 40 meV. The PDOS of both 2D and 3D TH-GY shows significant contributions from carbon *p*-orbitals near the Fermi level, supporting the intrinsic conductivity. The overlapping conduction and valence bands, combined with the high density of states at the Fermi level, indicate that TH-GY exhibits excellent electrical conductivity, a crucial property for high-performance anode materials in potassium-ion batteries. The porous structure, along with its metallic character, positions TH-GY as a strong candidate for high-capacity energy storage applications.

2D and 3D THGY as a potential anode material for K-ion batteries

To evaluate the potential of 2D and 3D TH-GY as an anode material for potassium-ion batteries (KIBs), we investigated relevant binding energy, storage capacity, and diffusion barrier for potassium ions. The binding energy of potassium ions on the TH-GY is a key factor in determining its suitability as an anode material for KIBs. Therefore, the adsorption energy of a single K-ion on the TH-GY surface was first assessed using the following relation:

$$E_{ads} = (E_{K+TH-GY} - E_{TH-GY} - nE_K)/n \quad (1)$$

where $E_{K+TH-GY}$ and E_{TH-GY} represent the total energies of potassium-adsorbed and pristine TH-GY, respectively, E_K is the energy of a single isolated potassium ion, and n denotes the total number of adsorbed potassium ions. As shown in figures 3 and 4, there are four stable adsorption sites of a single K-ion (S_1, S_2, S_3, and S_4) for 2D TH-GY and two stable adsorption sites (T, H) of a single K-ion on 3D TH-GY, and their corresponding adsorption energies are −1.15 eV, −0.97 eV, −1.27 eV, and −1.07 eV for 2D TH-GY, and −1.53 eV and −1.69 eV for 3D TH-GY, respectively. In this study, we also examined the adsorption parameters of 2D and 3D TH-GY for other ions, such as Li ion and Na ion. However, the results indicate that K ion adsorption is more stable and performs better than Li ion and Na ion. Thus, our primary focus of this study is put on K-ion systems. From the Bader charge analysis, we have determined the charge transfer between K-ion and TH-GY at all the selected adsorption sites, yielding the following values of 0.90, 0.93, 0.89, and 0.91,

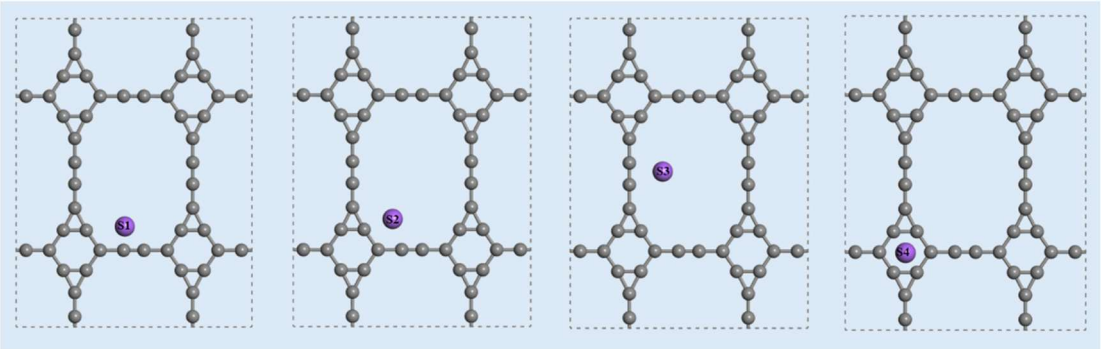

Figure 3. Four different sites suitable for the adsorption of K-ions for the geometrical symmetry of 2D TH-GY.

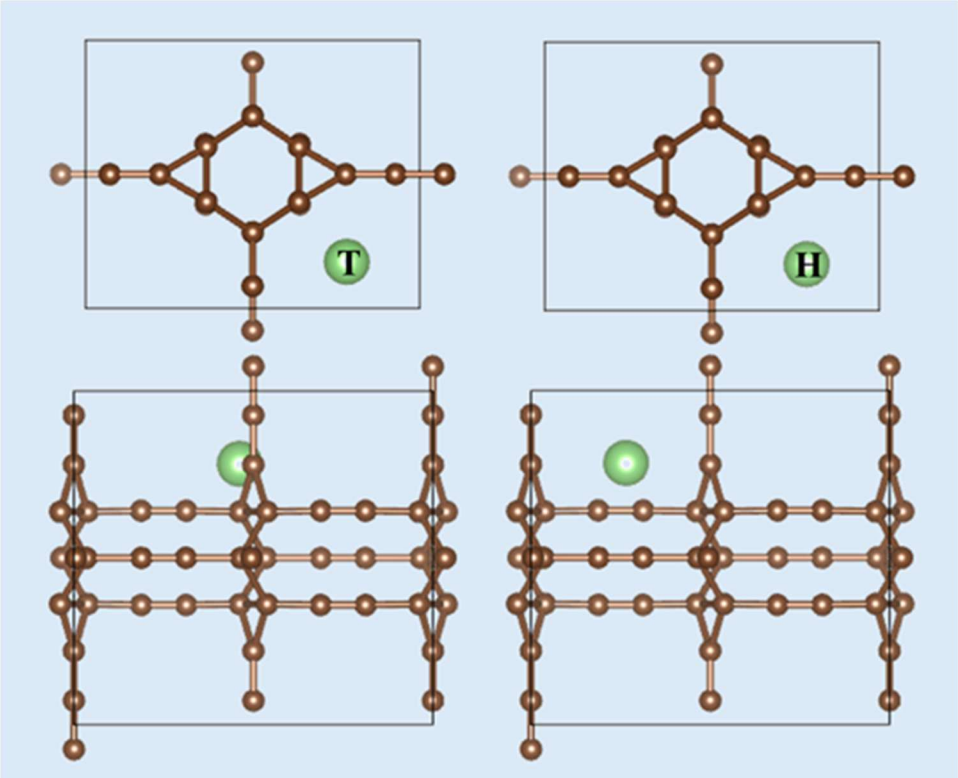

Figure 4. Two different sites suitable for the adsorption of K-ions for the geometrical symmetry of 3D TH-GY.

Table 1. Adsorption energies (E_{ads}) and Charge transfer (q) of a single K-ion at sites S1, S2, S3 and S4 of TH-GY.

System	2D TH-GY				3D TH-GY	
Sites	S1	S2	S3	S4	T	H
E_{ads} (eV)	−1.15	−0.97	−1.27	−1.07	−1.53	−1.69
q (|e|)	0.90	0.93	0.89	0.91	0.93	0.91

respectively. The charge transfers between K-ion and 3D-THGY at the two sites are 0.93 and 0.91, respectively. The results mentioned above are summarized in table 1.

To confirm the charge transfer of K-ions to 2D and 3D TH-GY at the most stable selected sites, we have calculated the charge density difference, a pictorial description of Bader charge analysis, which is computed using the equation: $\Delta\rho = \rho_{K+TH-GY} - \rho_{TH-GY} - n \cdot \rho_K$. Here, $\rho_{K+TH-GY}$ represents the total charge

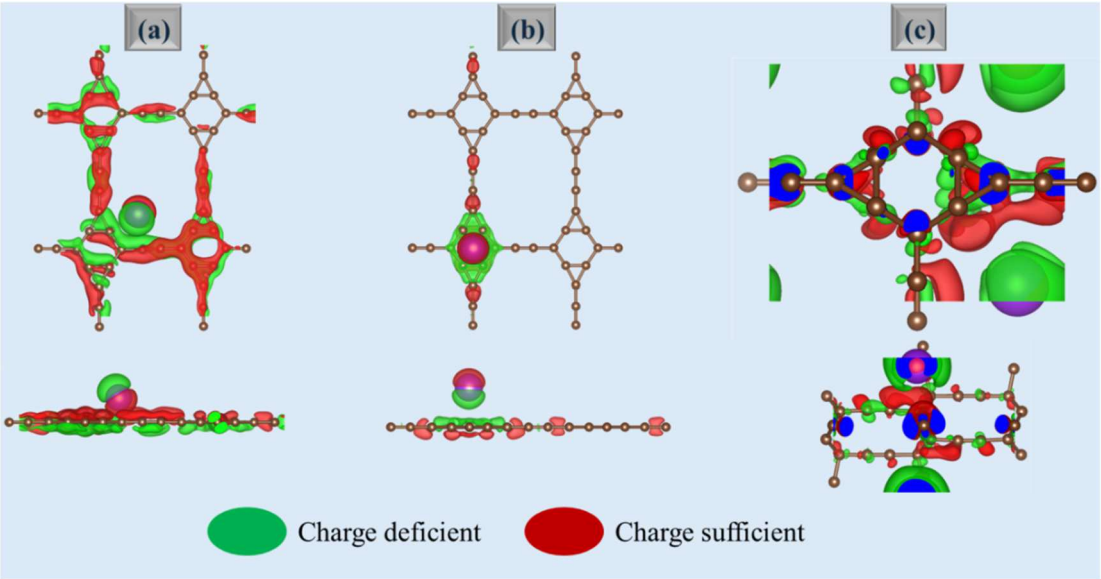

Figure 5. Charge density difference upon potassium adsorption at S2 (a) and S4 (b) sites of 2D TH-GY and T site of 3D TH-GY. Color coding shows charge transfer, whereas green and red colors indicate charge loss and gain, respectively.

density of the combined system where potassium (K) ions interact with the 2D/3D TH-GY material (i.e., the system after K ions transfer charge to TH-GY), ρ_{TH-GY} is the charge density of the pure TH-GY material (without any K ions present) and $n \cdot \rho_K$ is the charge density of an isolated K ion, while n is an integer that denotes the number of K ions. Results of the calculations are shown in figure 5. The green and red bubbles highlight the charge loss and charge gain regions for K-ions, respectively. The analysis revealed that electrons are mainly accumulated around carbon atoms, attributed to the higher electronegativity of carbon, compared to that of K-ions. To further understand the adsorption interaction between K-ions and TH-GY, we analyze the electronic band structure and partial density of states (PDOS) of K-ions adsorbed systems, results of which are given in Fig. S3. These results demonstrate how the interaction of K atoms with the TH-GY structure introduces additional states near the Fermi level, leading to enhanced metallicity and improved charge transport properties. Specifically, from the PDOS, we observe that the hybridization between the K orbitals and the carbon framework modifies the electronic band structure, facilitating efficient electron conduction and contributing to the system's overall electrochemical performance.

The rate performance of TH-GY as a potential high-performance anode material for K-ion batteries is determined based on the mobility of K-ions on our proposed substrate. The energy barrier for diffusion for K-ions in 2D and 3D TH-GY is obtained using the Climbing Image-Nudged Elastic Band (CI-NEB) method. According to the geometrical symmetry of 2D TH-GY, we have calculated the kinetics of K ions along the two different paths. In figures 6(a) and (b), we display path 1: S2 → S2 (orange arrow) for K-ion starting from the left corner of the biggest ring towards the right corner and Path 2: S4 → S4 (green arrow) from the bottom right towards top right along the *ab* plane. By employing the CI-NEB method, the diffusion barriers for path 1 and path 2 are 0.036 eV and 0.23 eV, respectively. The diffusion barrier for K-ion adsorbed at site S2 (0.036 eV) is lower than that of 3D-PGDY (0.100 eV) [45], blue-phosphorene (0.090 eV) [46], graphene (0.050 eV) [47], and other 2D carbon systems in table 2. The diffusion of K-ions on 3D TH-GY for the selected pathway is investigated [see figures 6(c) and (f)]. The pathways presented in the manuscript correspond to the most stable ones, exhibiting reasonable diffusion barriers. In figure 6(f), the energy barrier for the K-ion at the T-site in 3D TH-GY is shown along the c-direction. The calculated values of diffusion barriers are 0.19 eV for the T site and 0.24 eV for the H site, lower than that of borophene (0.62 eV) [48], and comparable to those of 3D PGDY [45] (0.10 eV) and Mo_2C (0.15 eV) [11]. The results indicate the fast charging/discharging ability of TH-GY for K-ion batteries. The calculated diffusion barriers of 0.036 eV for 2D TH-GY and 0.19 eV for 3D TH-GY indicate that potassium ions can migrate efficiently within these structures. Although the 3D framework presents a slightly higher diffusion barrier than its 2D counterpart, its improved stability and mechanical resilience offset this issue. This balance between ion mobility and structural integrity is essential for long-term cycling performance, reinforcing the potential of 3D TH-GY as a viable anode material for potassium-ion batteries. While the current NEB simulations focus on low potassium-ion concentrations to evaluate the fundamental migration pathways and energy barriers, it is important to note that higher K-ion concentrations could significantly influence the migration barriers due to Coulombic interactions and structural distortions. Future studies will

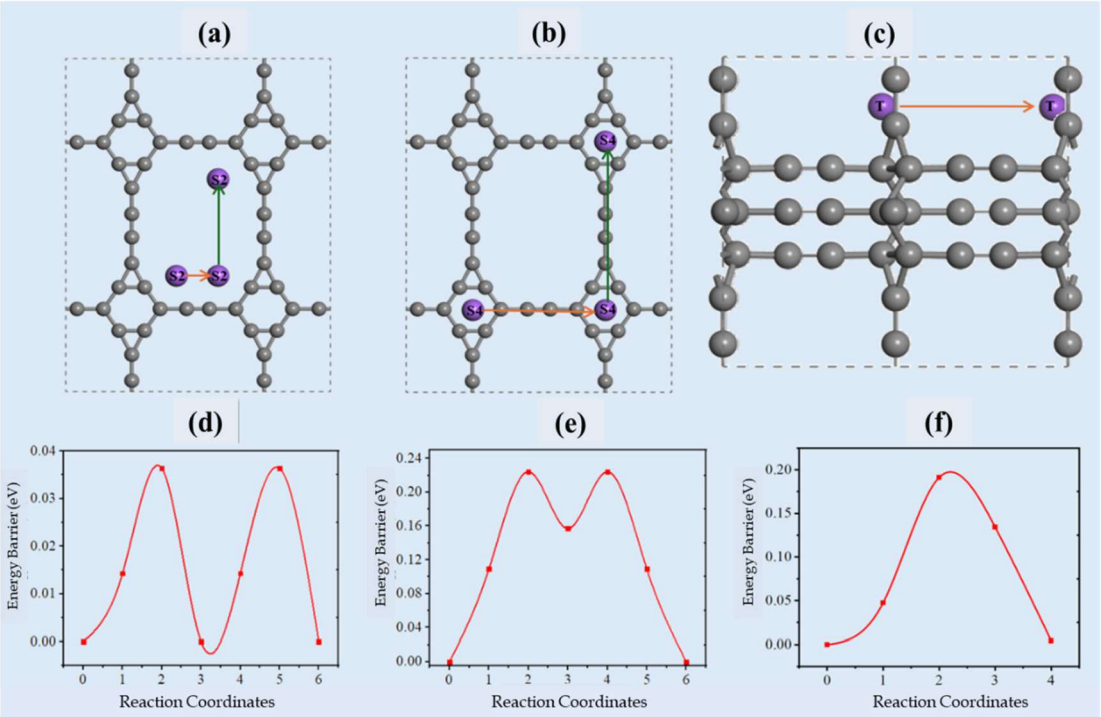

Figure 6. Diffusion pathway and energy barrier of K ions between equivalent adsorption sites S2 (a), (d) and S4 (b), (e) of 2D TH-GY and between equivalent adsorption sites T (c), (f) of 3D TH-GY.

Table 2. Comparative analysis of 2D and 3D materials regarding important parameters for metal ion batteries.

Systems	Capacity ($mAhg^{-1}$)	Migration (eV)	Voltage (V)	Electronic nature
3D TH-GY[a]	495.91	0.190	0.28	Semi-metallic
2D TH-GY[a]	929.93	0.036	0.30	Metallic
Graphite [18]	372	—	—	Metallic
B-doped Graphene [47]	564	0.050	0.20	Semi-metallic
Graphidyne [52]	744	0.150	0.25	Semi-conducting
Tet-C_{52} [55]	458	0.220	0.25	Semi-conducting
3D-TC_{60} [56]	706	0.110	0.24	Semi-conducting
MoS_2 [57]	220	0.200	0.80	Semiconducting
Ti_3C_2 [58]	800	0.100	0.40	Metallic
TPDH-graphene [59]	1116	0.08–0.20	0.29	Metallic
QPHT graphene [60]	837	0.36–0.83	0.66	Metallic
Pop-graphene [26]	1487	0.37–0.55	0.45	Metallic
2D-WS_2 [61]	334	0.48–0.42	—	Semi-conducting
3D-BPC_2 [62]	305.48	0.03	1.12	Metallic
3D-$TeTC_4$ [63]	627.6	0.09	0.27	Semi-conducting
HGY [64]	651	—	—	Semi-conducting
2D-$C_{18}H_6$ [65]	1449	0.125	0.28–0.024	Semi-conducting
3D-PC_6 [66]	520.26	0.22	0.58	Semi-conducting

[a] This work.

incorporate NEB simulations at higher concentrations to better understand the ion migration behavior under practical battery operating conditions.

The highest storage capacity for K-ion is obtained from the fully K-ion-loaded 2D and 3D TH-GY configurations, as shown in figures 7(a), (b). We calculated the theoretical capacities of both 2D and 3D TH-GY by progressively increasing the concentration of K ions on top of 2D TH-GY at S2 sites and at T sites of 3D TH-GY. As shown in figure 8(a), the binding energy steadily decreases. The theoretical capacity is obtained using equation (2):

$$C = nF/3.6M_{TH-GY} \quad (2)$$

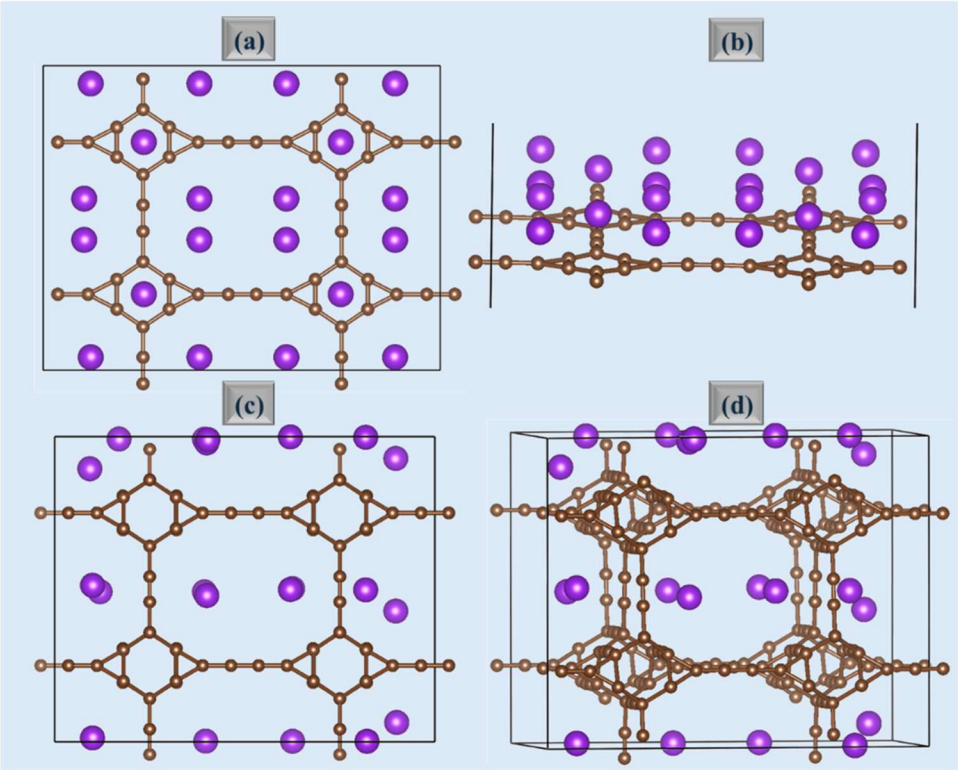

Figure 7. Top (a), (c) and side (b), (d) views of fully loaded K-ions on 2D and 3D TH-GY.

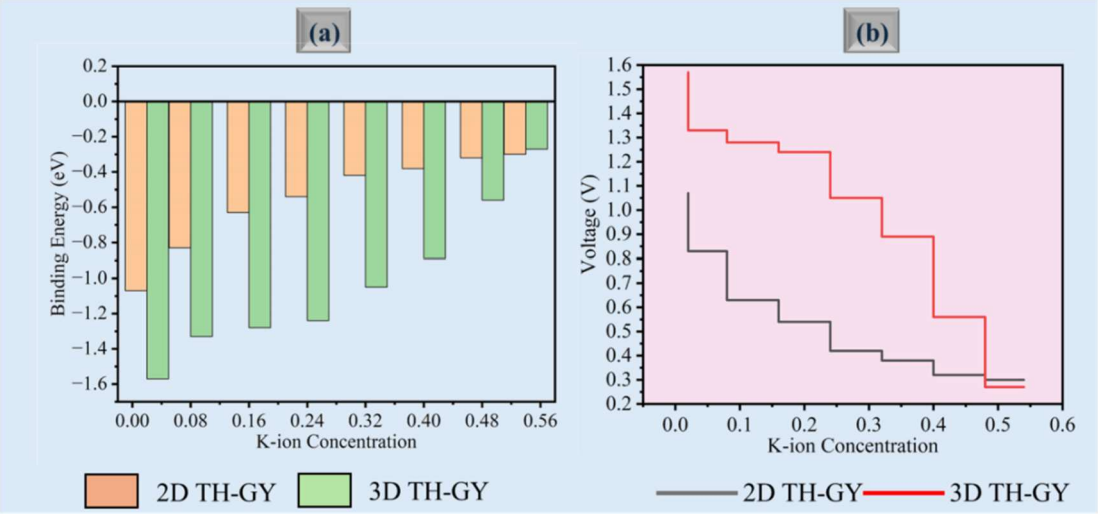

Figure 8. Changes in the binding energy (a) and variations in average voltage (b) with respect to the K-ions concentration for TH-GY.

where $n = 20$ denotes the number of K-ions adsorbed over the TH-GY surface, F is the Faraday constant (96485 sA mol^{-1}), and M is the molar mass of pristine. The maximum theoretical capacities obtained for the TH-GYs are 929.93 mAh g^{-1} and 495.91 mAh g^{-1}, which are higher than those of graphidyne [49], C_{60} [50], Mo_2C [11] and monolayer biphenylene [51, 52]. The performance of 3D TH-GY compares favorably with conventional graphite (372 mAh g^{-1}) [18] and graphidyne (744 mAh g^{-1}) [52], reaching a theoretical capacity of 495.91 mAh g^{-1}. Importantly, this capacity is achieved while preserving the structural robustness provided by its three-dimensional framework. Into-plane acetylene linkers enhance charge storage and ion diffusion without compromising mechanical stability, making 3D TH-GY a promising alternative for potassium-ion battery anodes. Moreover, the volume expansion was calculated, which is one of the causes of the degradation

of batteries. The volume changes for maximum adsorption in 3D-TH-GY is 6.4% for K-ions, which is comparable to the volume expansion for K-ions in BDL-14 [53] (7.0%) and 3D-β_{12}-borophene (7.4%) [54].

It may need to mention that in the calculation of the theoretical capacity, 20 K-ions were chosen as the maximum. The reason is given based on the adsorption energy, which is a key indicator of the stability of ion's adsorption into a material. When the adsorption energy becomes positive during an adsorption process, the system becomes unable to adsorb further metal ions. In our case when more than 20 K-ions are adsorbed, the adsorption energy turns positive, which reveals the saturation state of the system, implying that the process starts to become energetically unfavorable now.

Figure 8 depicts the potential interaction between K atoms. This interaction influences the electronic properties of the system. We have included the electronic band structure and PDOS of K atoms adsorbed systems in the Supplementary information (see figure S3). These results demonstrate how the interaction of K atoms with the TH-GY structure introduces additional states near the Fermi level, leading to enhanced metallicity and improved charge transport properties. Specifically, from the PDOS, one may see that the hybridization between the K orbitals and the carbon framework modifies the electronic band structure, facilitating efficient electron conduction and contributing to the system's overall electrochemical performance.

As shown in figure 8(a), the binding energy steadily decreases with increasing potassium-ion concentration, confirming the effective adsorption capability of 3D TH-GY. At low K-ion coverage, the strong interaction between potassium and the porous framework ensures stable adsorption, a key feature for efficient anode materials. As the K-ion concentration increases, Coulombic repulsion between adsorbed ions gradually reduces binding energy. This behavior is consistent with other carbon-based anode materials [48, 56]. It indicates that 3D TH-GY can accommodate a high K-ion load while maintaining structural integrity, an essential requirement for practical applications. To assess the open circuit voltage (OCV), a critical parameter for evaluating the performance of metal-ion batteries, the average voltage of TH-GY as a function of K-ions concentration, was calculated using the relationship $V = -(E_{n\cdot K+TH-GY} - E_{TH-GY} - nE_K)/ne$, where $E_{n\cdot K+TH-GY}$ and E_{TH-GY} represent the total energies of potassium-adsorbed and pristine TH-GY, respectively, and E_K is the energy of each potassium ion. n denotes the number of potassium ions adsorbed on 2D and 3D TH-GY structures. The average voltages of metallic 2D and 3D TH-GY systems for K-ions vary with different concentrations of potassium ions. We calculated the voltage plateau for six different concentrations, as shown in figure 8(b). As the concentrations of K-ions increase, a gradual decrease in voltage is observed due to the repulsion between the K-ions. In contrast, the repulsion between the K-ions and the C-atoms in TH-GY remains relatively low. The average voltages are calculated as 0.30 V and 0.28 V for 2D and 3D TH-GY, respectively, as the targeted voltages for energy storage systems. At low potassium-ion concentrations, the voltage is initially high for 2D and 3D TH-GY, indicating a significant potential difference between the anode and cathode. This is attributed to the strong interaction between K-ions and the TH-GY anodes. As the K-ion concentration increases, a step-like plateau region is observed in the voltage profile, especially for 3D TH-GY, suggesting stable phase transitions during ion intercalation. The relatively smaller voltage variation in this region reflects the structural resilience and uniform ion adsorption capability of the TH-GY frameworks. At higher concentrations approaching full saturation, the voltage begins to decrease, signifying that the adsorption sites within the anode are becoming fully occupied, thereby reducing the energy required for further K-ion intercalation. The higher initial voltage and extended plateau in 3D TH-GY, compared to those of 2D TH-GY, demonstrate its superior ability to accommodate larger K-ion loads, likely due to its enhanced porosity and structural flexibility. To further highlight the anode performance of TH-GY, compared to other 2D and 3D systems, the obtained results are summarized in table 2.

4. Conclusions

In summary, for the first time, we have designed a 3D Triangular-Hexagonal-Graphyne (semi-metallic), following the geometrical pattern of 2D TH-GY. This novel 3D allotrope TH-GY comprises 3–6 carbon rings, showing exceptional stability and intrinsic semi-metallicity. First-principles calculations are performed on the TH-GY-based carbon structure to assess its compatibility as a positive electrode for potassium-ion batteries. The structure offers multiple adsorption sites for K ions, leading to (1) high theoretical capacities of 929.9 $mAhg^{-1}$ for 2D TH-GY and 495.91 $mAhg^{-1}$ for 3D TH-GY, respectively; (2) ultra-small diffusion barriers of 0.03 eV and 0.22 eV for 2D TH-GY and 0.19 eV for 3D TH-GY, respectively; and (3) low average voltages of 0.30 V and 0.28 V for 2D and 3D TH-GYs, respectively. The results reveal that TH-GY outperforms the previously studied 3D carbon allotropes such as graphidyne, C_{60}, and 3D-PGDY. We anticipate that this study will not only inspire experimental efforts on synthesizing TH-GY-based carbon materials but also pave the way to explore universal carbon-based materials for high-performance K-ion batteries.

Acknowledgments

The authors are grateful for financial support from the Centre for Energy and Mineral Processing (UOFAB Li), Trimay Wear Plate Ltd., Suncor Energy (TWPL Li), and Digital Research Alliance of Canada. M.L.P.J. acknowledges financial support from the Research Support Foundation of the Federal District (FAP-DF, grant 00193-00001807/2023-16) and the National Council for Scientific and Technological Development (CNPq, grant 444921/2024-9).

Data availability statement

All data that support the findings of this study are included within the article (and any supplementary files).

Author contributions

Arzoo Hassan 0000-0001-5593-0473
Conceptualization (equal), Data curation (equal), Formal analysis (equal), Investigation (equal), Validation (equal), Writing – original draft (lead)

Marcelo L Pereira Junior 0000-0001-9058-510X
Conceptualization (equal), Methodology (equal), Resources (equal), Validation (equal)

L Shaw
Conceptualization (equal), Methodology (equal), Resources (equal), Validation (equal)

Umer Younis 0000-0002-5857-0693
Methodology (equal), Resources (equal), Validation (equal)

Dongyang Li 0000-0002-6285-2968
Conceptualization (equal), Formal analysis (equal), Methodology (equal), Resources (lead), Funding acquisition (lead), Validation (equal), Writing – review & editing (lead)

References

[1] Kumar R, Singh M and Soam A 2020 Study on electrochemical properties of silicon micro particles as electrode for supercapacitor application *Surfaces and Interfaces* **19** 100524
[2] Zhao C, Song Y, Chen H, Chen H, Li Y, Lei A, Wu Q and Zhu L 2025 Improving the performance of microbial fuel cell stacks via capacitive-hydrogel bioanodes *Int. J. Hydrogen Energy* **97** 708–17
[3] Huang W, Sun Y, Zhao G, Liu Q, Zhao G, Duan L, An Q, Ren F, Sun M and Xia S 2024 Constructing nano spinel phase and Li+ conductive network to enhance the electrochemical stability of ultrahigh-Ni cathode *Mater. Today* **79** 86–96
[4] Wang C and Chen Y 2024 Unsupervised dynamic prognostics for abnormal degradation of lithium-ion battery *Appl. Energy* **365** 123280
[5] Liu L, Zhu L, Wang Y, Guan X, Zhang Z, Li H, Wang F, Zhang H, Zhang Z and Yang Z 2025 Starfish-inspired solid-state Li-ion conductive membrane with balanced rigidity and flexibility for ultrastable lithium metal batteries *Angew. Chem. Int. Ed.* **64** e202420001
[6] Di Giorgio P, Di Ilio G, Jannelli E and Conte F V 2023 Numerical analysis of an energy storage system based on a metal hydride hydrogen tank and a lithium-ion battery pack for a plug-in fuel cell electric scooter *Int. J. Hydrogen Energy* **48** 3552–65
[7] Niu B, Xu Z, Xiao J and Qin Y 2023 Recycling hazardous and valuable electrolyte in spent lithium-ion batteries: urgency, progress, challenge, and viable approach *Chem. Rev.* **123** 8718–35
[8] Wang Y, Chen R, Chen T, Lv H, Zhu G, Ma L, Wang C, Jin Z and Liu J 2016 Emerging non-lithium ion batteries *Energy Storage Mater.* **4** 103–29
[9] Du J, Lin H and Huang Y 2023 Metallic BSi3 monolayer as a high rate-capacity anode material for flexible potassium ion batteries: a first-principles study *FlatChem* **42** 100551
[10] Que L and Chen W 2024 Research on the thermo-electrochemical behavior during the electrodeposition process of lithium metal battery *Int. J. Hydrogen Energy* **49** 1101–20
[11] Çakır D, Sevik C, Gülseren O and Peeters F M 2016 Mo 2 C as a high capacity anode material: A first-principles study *J. Mater. Chem. A* **4** 6029–35
[12] Lu S Y, Jin M, Zhang Y, Niu Y B, Gao J C and Li C M 2018 Chemically exfoliating biomass into a graphene-like porous active carbon with rational pore structure, good conductivity, and large surface area for high-performance supercapacitors *Adv. Energy Mater.* **8** 1702545
[13] Paquin F, Rivnay J, Salleo A, Stingelin N and Silva C 2013 Multi-phase semicrystalline microstructures drive exciton dissociation in neat plastic semiconductors arXiv:1310.8002
[14] Wang J-T, Chen C and Mizuseki H 2020 Body centered cubic carbon BC14: an all-sp 3 bonded full-fledged pentadiamond *Phys. Rev. B* **102** 184106

[15] Tromer R M, Felix L C, Woellner C F and Galvao D S 2021 A DFT investigation of the electronic, optical, and thermoelectric properties of pentadiamond *Chem. Phys. Lett.* **763** 138210
[16] Li Z, Wu Y, Zhang S, Zhang Y, Gao Y, Luo K, Zhao Z and He J 2020 Pentadiamond-like metallic hard carbon nitride *The Journal of Physical Chemistry C* **124** 24978–83
[17] Chane-Ching J Y, Cobo F, Aubert D, Harvey H G, Airiau M and Corma A 2005 A general method for the synthesis of nanostructured large-surface-area materials through the self-assembly of functionalized nanoparticles *Chemistry–A European Journal* **11** 979–87
[18] Liu J, Wang S and Sun Q 2017 All-carbon-based porous topological semimetal for Li-ion battery anode material *Proc. Natl Acad. Sci.* **114** 651–6
[19] Younis U, Muhammad I, Qayyum F, Wu W and Sun Q 2021 Two-dimensional metallic pentadiamond as anode material for Li-/Na-/K-ion batteries with high performance *Materials Today Energy* **20** 100664
[20] Younis U, Qayyum F, Ahmad W, Hassan A, Singh N, Yaseen M, Zhang Y and Wang Z 2024 Two-dimensional azulenoid kekulene-based metallic allotropes for energy storage applications *J. Mater. Chem. A* **12** 32972–80
[21] Wang X, Feng Z, Rong J, Zhang Y, Zhong Y, Feng J, Yu X and Zhan Z 2019 Planar net-τ: a new high-performance metallic carbon anode material for lithium-ion batteries *Carbon* **142** 438–44
[22] Zheng F, Yang Y and Chen Q 2014 High lithium anodic performance of highly nitrogen-doped porous carbon prepared from a metal-organic framework *Nat. Commun.* **5** 5261
[23] Sun C and Searles D J 2012 Lithium storage on graphdiyne predicted by DFT calculations *The Journal of Physical Chemistry C* **116** 26222–6
[24] Yu S, Rao Y-C, Li S-F and Duan X-M 2018 Net W monolayer: a high-performance electrode material for Li-ion batteries *Appl. Phys. Lett.* **112**
[25] Younis U, Muhammad I, Kawazoe Y and Sun Q 2020 Design of tetracene-based metallic 2D carbon materials for Na-and K-Ion batteries *Appl. Surf. Sci.* **521** 146456
[26] Wang S, Yang B, Chen H and Ruckenstein E 2018 Popgraphene: a new 2D planar carbon allotrope composed of 5–8–5 carbon rings for high-performance lithium-ion battery anodes from bottom-up programming *J. Mater. Chem. A* **6** 6815–21
[27] Martins N F, Laranjeira J A, Fabris G S, Denis P A and Sambrano J R 2024 Irida-graphene as a high-performance anode for sodium batteries *Journal of Energy Storage* **104** 114637
[28] Hu J, Ouyang C, Yang S A and Yang H Y 2019 Germagraphene as a promising anode material for lithium-ion batteries predicted from first-principles calculations *Nanoscale Horizons* **4** 457–63
[29] Khoo K H, Neaton J, Son Y W, Cohen M L and Louie S G 2008 Negative differential resistance in carbon atomic wire-carbon nanotube junctions *Nano Lett.* **8** 2900–5
[30] Nguyen K T, Gaur A and Shim M 2007 Fano lineshape and phonon softening in single isolated metallic carbon nanotubes *Phys. Rev. Lett.* **98** 145504
[31] McKee D W 1974 Effect of metallic impurities on the gasification of graphite in water vapor and hydrogen *Carbon* **12** 453–64
[32] Lu S, Liu H, Naumov I I, Meng S, Li Y, Tse J S, Yang B and Hemley R J 2016 Superconductivity in dense carbon-based materials *Phys. Rev. B* **93** 104509
[33] Fan Q, Yan L, Tripp M W, Krejčí O, Dimosthenous S, Kachel S R, Chen M, Foster A S, Koert U and Liljeroth P 2021 Biphenylene network: a nonbenzenoid carbon allotrope *Science* **372** 852–6
[34] Ullah S, Menezes M G and Silva A M 2024 Theoretical characterization of tolanene: a new 2D sp-sp2 hybridized carbon allotrope *Carbon* **217** 118618
[35] Jenkins T, Silva A M, Menezes M G, Thonhauser T and Ullah S 2024 Thd-c sheet: a novel nonbenzenoid carbon allotrope with tetra-, hexa-, and dodeca-membered rings *The Journal of Physical Chemistry C* **128** 10982–96
[36] Lima K A, Alves R A, da Silva D A, Mendonça F L, Pereira M L and Ribeiro L A 2025 TH-graphyne: a new porous bidimensional carbon allotrope *Phys. Chem. Chem. Phys.* **27** 8684–91
[37] Hassan A, Guo Y, Wang Q, Kawazoe Y and Jena P 2019 Interfacial properties of penta-graphene-metal contacts *J. Appl. Phys.* **125** 065308
[38] Ernzerhof M and Scuseria G E 1999 Assessment of the perdew–burke–ernzerhof exchange-correlation functional *J. Chem. Phys.* **110** 5029–36
[39] Śpiewak P and Kurzydłowski K J 2013 Formation and migration energies of the vacancy in Si calculated using the HSE06 range-separated hybrid functional *Physical Review B—Condensed Matter and Materials Physics* **88** 195204
[40] Dral P O, Wu X, Spörkel L, Koslowski A, Weber W, Steiger R, Scholten M and Thiel W 2016 Semiempirical quantum-chemical orthogonalization-corrected methods: theory, implementation, and parameters. *J. Chem. Theory Comput.* **12** 1082–96
[41] Allouche A R 2011 Gabedit—a graphical user interface for computational chemistry softwares *J. Comput. Chem.* **32** 174–82
[42] Henkelman G, Uberuaga B P and Jónsson H 2000 A climbing image nudged elastic band method for finding saddle points and minimum energy paths *J. Chem. Phys.* **113** 9901–4
[43] Andersson D and Beeler B W 2022 *Ab initio* molecular dynamics (AIMD) simulations of NaCl, UCl3 and NaCl-UCl3 molten salts *J. Nucl. Mater.* **568** 153836
[44] Qi R, Shi R, Li Y, Sun Y, Wu M, Li N, Du J, Liu K, Chen C and Chen J 2021 Measuring phonon dispersion at an interface *Nature* **599** 399–403
[45] Muhammad I, Younis U, Wu W, Xie H, Khaliq A and Sun Q 2020 Three-dimensional porous phosphorus-graphdiyne as a universal anode material for both K-and Ca-ion batteries with high performance *J. Power Sources* **480** 228876
[46] Mukherjee S, Kavalsky L and Singh C V 2018 Ultrahigh storage and fast diffusion of Na and K in blue phosphorene anodes *ACS Appl. Mater. Interfaces* **10** 8630–9
[47] Gong S and Wang Q 2017 Boron-doped graphene as a promising anode material for potassium-ion batteries with a large capacity, high rate performance, and good cycling stability *The Journal of Physical Chemistry C* **121** 24418–24
[48] Xiang P, Chen X, Zhang W, Li J, Xiao B, Li L and Deng K 2017 Metallic borophene polytypes as lightweight anode materials for non-lithium-ion batteries *Phys. Chem. Chem. Phys.* **19** 24945–54
[49] Zhang H, Xia Y, Bu H, Wang X, Zhang M, Luo Y and Zhao M 2013 Graphdiyne: a promising anode material for lithium ion batteries with high capacity and rate capability *J. Appl. Phys.* **113** 044309
[50] Gorelik R, Asaduzzaman A, Manga V R, Thakur A and Muralidharan K 2022 A first-principles investigation of lithium and sodium ion diffusion in C60 molecular solids *The Journal of Physical Chemistry C* **126** 4259–66
[51] Kaur M, Duhan N and Kumar T D 2024 N-doped biphenylene monolayer as high-performance 2D electrode material for Li-ion batteries *Journal of Energy Storage* **94** 112353

[52] Li J, Yi Y, Zuo X, Hu B, Xiao Z, Lian R, Kong Y, Tong L, Shao R and Sun J 2022 Graphdiyne/graphene/graphdiyne sandwiched carbonaceous anode for potassium-ion batteries *ACS nano* **16** 3163–72
[53] Li X, Liu J, Wang F Q, Wang Q and Jena P 2019 Rational design of porous nodal-line semimetallic carbon for K-ion battery anode materials *The Journal of Physical Chemistry Letters* **10** 6360–7
[54] Muhammad I, Younis U, Xie H, Khan A A, Khaliq A, Samad A, Schwingenschlogl U and Sun Q 2021 Borophene-based three-dimensional porous structures as anode materials for alkali metal-ion batteries with ultrahigh capacity *Chem. Mater.* **33** 2976–83
[55] Obeid M M and Sun Q 2022 Assembling biphenylene into 3D porous metallic carbon allotrope for promising anode of lithium-ion batteries *Carbon* **188** 95–103
[56] Younis U, Qayyum F, Muhammad I, Yaseen M and Sun Q 2022 A Stable three-dimensional porous carbon as a high-performance anode material for lithium, sodium, and potassium ion batteries *Advanced Theory and Simulations* **5** 2200230
[57] Rehman J, Fan X, Laref A, Dinh V A and Zheng W 2021 Potential anodic applications of 2D MoS2 for K-ion batteries *J. Alloys Compd.* **865** 158782
[58] Fatima S A and Park J 2024 Two-dimensional carbon rich titanium carbide (TiC3) as a high-capacity anode for potassium ion battery *Appl. Surf. Sci.* **659** 159879
[59] Gomez Quispe J, Ipaves B, Galvao D S and Autreto P A d S 2024 Tpdh-graphene as a new anodic material for lithium ion battery: Dft-based investigations *ACS omega* **9** 39195–201
[60] Qiu T-C, Shao Z-G, Wang C-L and Yang L 2022 QPHT graphene as a high-performance lithium ion battery anode materials with low diffusion barrier and high capacity *Phys. Lett. A* **456** 128549
[61] Sengupta S, Pramanik A, de Oliveira C C, Chattopadhyay S, Pieshkov T, Autreto P A d S, Ajayan P M and Kundu M 2024 Deciphering sodium-ion storage: 2D-sulfide versus oxide through experimental and computational analyses *Small* **20** 2403321
[62] Younis U, Muhammad I, Qayyum F, Kawazoe Y and Sun Q 2020 A stable metallic 3D porous BPC 2 as a universal anode material for Li, Na, and K ion batteries with high performance *J. Mater. Chem. A* **8** 25824–30
[63] Younis U, Qayyum F, Ahmad W, You M, Hassan A, Manasa P, Mohammed M A, Rehman J, Zhang Y and Wang Z 2025 Exploring stable 3D porous carbon for advanced optoelectronics and electrochemical performance in potassium-ion batteries *J. Power Sources* **644** 237080
[64] Jeon T, Lee Y C and Jung S C 2025 Holey graphyne anode for metal-ion batteries: suitability for potassium-ion batteries *Nanoscale* **17** 15924–34
[65] Jiang J, Guo H, Zhang J, Zuo G Z, Wu X, Zhuo Z and Lu N 2023 Poly-triphenylene membrane: a multifunctional two-dimensional porous carbon framework with ultra-high carrier mobilities and potassium ion storage capacity *Appl. Surf. Sci.* **631** 157503
[66] Younis U, Qayyum F, Hassan A, Singh N, Ahmad W, Channa A I, Rehman J, Manasa P, Zhang Y and Wang Z 2024 Rational design of 3D porous phosphorus-carbide with excellent optical performance and energy storage application *J. Power Sources* **612** 234783